14th International Conference on Information Fusion
Chicago, Illinois, USA, July 5-8, 2011

Target Positioning and Tracking in Degenerate Geometry

Chun Yang
Sigtem Technology, Inc.
San Mateo, CA 94402
chunynag@sigtem.com

Lance Kaplan
ARL/SEDD
Adelphi, MD 20783
lance.m.kaplan@us.army.mil

Erik Blasch
AFRL/RYAA
WPAFB, OH 45433
erik.blasch@wpafb.afb.mil

Michael Bakich
AFRL/RYAA
WPAFB, OH 45433
michael.bakich@wpafb.af.mil

Abstract - This paper analyzes the effects of special target-sensor geometries, particularly, some degenerate cases (near singular observation matrix), on the performance of target positioning and tracking. A scenario of practical significance is when two or more sensors form nearly parallel line of sight (LOS) vectors to targets. Examples include netted radars that happen to line up their observations in azimuth. Such encounter geometry is degenerate for conventional methods. In this paper, we first analyze conventional estimates in such degenerate geometry and then describe three adapted methods, namely, a geometric 1D solution for 2D scenarios, a reduced-order least squares method, and a subspace least squares method. Simulation results are presented to compare the methods. The analysis provides the basis for active sensor management performance prediction and optimization via sensor placement/ assignment.

Keywords: Target tracking, Degenerate geometry, Active sensor management, Performance prediction

1. Introduction

The estimation accuracy of a target positioning and tracking system is determined by two factors. One is the errors in target measurements (ranges, bearings, or both). The other is the geometry between the targeting sensors and the target, which is captured in the observation matrix made of line of sight (LOS) vectors. One way to characterize the effect of geometry on estimation accuracy is to use the geometric dilution of precision (GDOP) [8]. In a poor geometry with not enough independent measurements and/or nearly collinear LOS vectors, the observation matrix is ill-conditioned, which presents a numerical difficulty to invert the solution matrix. The poor geometry not only inflates the variance of the position estimates but also amplifies any biases that may be present in the measurements [9].

A particular scenario of practical significance is when two or more sensors form nearly parallel LOS vectors to targets. Examples include co-located sensors and bistatic radars that happen to line up in azimuth. Such scenarios also occur in other applications such as narrow sky view of GPS satellites in urban canyons and radio beacons along a corridor and cell phone towers along a freeway. These degenerate geometries are detrimental to positioning.

Several methods have been used in the literature to bound estimation errors. For a rank-deficient observation matrix, the null space is not empty and the solution is not unique and one way to solve the problem is to place constraints on the solution. A circular restriction (or a spherical constraint) leads to the so-called *ridge regression* [1, 3]. A more general formulation is *Tikhonov regularization*, which includes a constraint term on the solution (i.e., a penalty on each variable) in addition to the measurement error term in the performance index, which is also referred to the *regularized least squares* (RLS) [5]. Other means can be used to obtain similar results, including heuristic *diagonal loading*, use of prior knowledge such as road information [6, 7], and use of prior knowledge as fictitious measurements [4].

In Sect. 2, we first present an analysis of conventional estimates in degenerate geometry. Next, in Sect. 3, we set forth three methods adapted to singular geometry, namely, a geometric 1D solution for 2D scenarios, a reduced-order least squares method, and a subspace least squares method. In Sect. 4, we present comparative simulation results of the methods with analysis. Finally we conclude the paper with a summary and future work and its implication for active sensor placement and adaptive resource management.

2. Regular Methods in Degenerate Geometry

The maximum likelihood estimate (MLE) is derived and analyzed in degenerate geometry.

2.1 Maximum Likelihood Estimate

Consider two sensors located at $\mathbf{s}_1$ and $\mathbf{s}_2$. Both detect the same target located at $\mathbf{t}$. The range measurements are denoted by:

$$r_i = \|\mathbf{t} - \mathbf{s}_i\|_2 + n_i \quad (1)$$

where n_i is an independent zero-mean Gaussian noise with varaince σ_i^2 for $i = 1$ and 2.

For a possible target location estimate at $\mathbf{x}$, the un-normalzied likelihood surface is given by:

$$L(\mathbf{x}) = \prod_{i=1}^{2} \exp\left(-\frac{1}{2}\frac{(r_i - \|\mathbf{x} - \mathbf{s}_i\|_2)^2}{\sigma_i^2}\right) \quad (2)$$

The maximum likelihood estimate is given by:

$$\hat{\mathbf{x}}_{ML} = \arg\max_{\mathbf{x}}\{L(\mathbf{x})\} \quad (3)$$

It is clear from (3) that the maximum is reached when the exponential arguments are zero. It is equivalent to finding the intersection of two circles as:

$$r_i - \|\mathbf{x} - \mathbf{s}_i\|_2 = 0,\ i = 1, 2 \quad (4)$$

Report Documentation Page

Form Approved
OMB No. 0704-0188

1. REPORT DATE	2. REPORT TYPE	3. DATES COVERED
JUL 2011		**00-00-2011 to 00-00-2011**

4. TITLE AND SUBTITLE	5a. CONTRACT NUMBER
Target Positioning and Tracking in Degenerate Geometry	5b. GRANT NUMBER
	5c. PROGRAM ELEMENT NUMBER
6. AUTHOR(S)	5d. PROJECT NUMBER
	5e. TASK NUMBER
	5f. WORK UNIT NUMBER
7. PERFORMING ORGANIZATION NAME(S) AND ADDRESS(ES) **Army Research Laboratory,ARL/SEDD,Adelphi,MD,20783**	8. PERFORMING ORGANIZATION REPORT NUMBER
9. SPONSORING/MONITORING AGENCY NAME(S) AND ADDRESS(ES)	10. SPONSOR/MONITOR'S ACRONYM(S)
	11. SPONSOR/MONITOR'S REPORT NUMBER(S)

12. DISTRIBUTION/AVAILABILITY STATEMENT
Approved for public release; distribution unlimited

13. SUPPLEMENTARY NOTES
Presented at the 14th International Conference on Information Fusion held in Chicago, IL on 5-8 July 2011. Sponsored in part by Office of Naval Research and U.S. Army Research Laboratory.

14. ABSTRACT
This paper analyzes the effects of special target-sensor geometries, particularly, some degenerate cases (near singular observation matrix), on the performance of target positioning and tracking. A scenario of practical significance is when two or more sensors form nearly parallel line of sight (LOS) vectors to targets. Examples include netted radars that happen to line up their observations in azimuth. Such encounter geometry is degenerate for conventional methods. In this paper, we first analyze conventional estimates in such degenerate geometry and then describe three adapted methods, namely, a geometric 1D solution for 2D scenarios, a reduced-order least squares method, and a subspace least squares method. Simulation results are presented to compare the methods. The analysis provides the basis for active sensor management performance prediction and optimization via sensor placement/ assignment.

15. SUBJECT TERMS

16. SECURITY CLASSIFICATION OF:			17. LIMITATION OF ABSTRACT	18. NUMBER OF PAGES	19a. NAME OF RESPONSIBLE PERSON
a. REPORT **unclassified**	b. ABSTRACT **unclassified**	c. THIS PAGE **unclassified**	**Same as Report (SAR)**	**8**	

Without loss of generality, assume that sensor 1 is located at (x_1, 0) and sensor 2 at (-x_1, 0), as shown in Fig. 1. We now consdier three cases.

Case 1: $r_1 + r_2 \geq 2x_1$. In this case, use of range measurements of r_1 and r_2 leads to the following estimate:

$$\hat{x} = \frac{r_2^2 - r_1^2}{4x_1} \tag{5a}$$

$$\hat{y}_+ = \sqrt{\frac{4r_1^2 r_2^2 - (4x_1^2 - (r_1^2 + r_2^2))^2}{16x_1^2}} \tag{5b}$$

$$\hat{y}_- = -\sqrt{\frac{4r_1^2 r_2^2 - (4x_1^2 - (r_1^2 + r_2^2))^2}{16x_1^2}} \tag{5c}$$

as long as the range variance is equal for both sensors.

For ranging sensors, unlike bearings sensors, an ambiguous solution exists, arising from the intersection of two circles. However, if the target has been tracked, the ambiguity is resolved (knowing which side of the baseline the target lies).

Case 2: $r_1 + r_2 = 2x_1$. In this case, it can be seen from (5b) and (5c) that $\hat{y} = 0$, which is the so-called degenerate case in which the LOS vectors are parallel. The Fisher information matrix (FIM) for the two ranging sensors with a target on the baseline of the sensors is singular. This would indicate that the localization algorithm becomes degenerate. Eq. (5a) can be further written as:

$$\hat{x} = \frac{r_2^2 - r_1^2}{4x_1} = \frac{(r_2 - r_1)(r_2 + r_1)}{4x_1} = \frac{r_2 - r_1}{2} \tag{6}$$

In general, for two sensors located at x_1 and x_2 along the x-axis with their range measurements r_1 and r_2 to a target also on the x-axis. Then an intuitive solution constrained on the baseline ($\bar{y} = 0$) is the average of the two measurements given by:

$$x_1 - \bar{x} = r_1 \tag{7a}$$

$$\bar{x} - x_2 = r_2 \tag{7b}$$

Subtracting (7b) from (7a) gives:

$$\bar{x} = \frac{x_1 + x_2}{2} + \frac{r_2 - r_1}{2} \tag{8a}$$

$$= \frac{r_2 - r_1}{2}, \text{ if } x_1 = -x_2 \tag{8b}$$

The intuitive averaging (8) is the same as the MLE (6) if $r_1 + r_2 = 2x_1$, which is also Method 1 discussed in Section 3.1.

Case 3: $r_1 + r_2 < 2x_1$. In this case, the circles do not intercept as shown in Fig. 2. There are four possible solutions:

Solution 1 from (5a): ($\hat{x}$, 0), abbreviated as "sect" (9a)

Solution 2: ($\hat{x}_+ = x_1 - r_1$, 0), "posi" (9b)

Solution 3: ($\hat{x}_- = -x_1 + r_2$, 0), "nega" (9c)

Solution 4 from (8b): ($\bar{x}$, 0), "ave" (9d)

Note that the average of Solutions 2 and 3 is Solution 4:

$$\frac{\hat{x}_+ + \hat{x}_-}{2} = \frac{(x_1 - r_1) + (-x_2 + r_2)}{2} = \frac{r_2 - r_1}{2} = \bar{x} \sim \hat{x} \tag{10}$$

In this case, it can be seen from the geometry of Fig. 2 that the ML estimate occurs on the baseline and in the middle of two measurements, denoted by $\hat{x}_A$.

To prove this, we take two steps. First, for all possible estimates on the baseline, we will show that the one in the middle of two mesurements, $\hat{x}_A$, maximizes the likelihood function (2). Denote the measurement prediction error by

$$\Delta r_i = r_i - \| \hat{\mathbf{x}} - \mathbf{s}_i \|_2, \; i = 1, 2 \tag{11}$$

Then maximizing the likelihood function (2) is equivent to minimizing the log likelohood as:

$$l(\hat{\mathbf{x}}) = -2\sigma^2 \ln(L(\hat{\mathbf{x}})) = \Delta r_1^2 + \Delta r_2^2 \tag{12}$$

Insepecting Fig. 2 reveals the following constraint:

$$\Delta r_1 + \Delta r_2 = 2x_1 - (r_1 + r_2) = c \tag{13}$$

where c is a constant for the given measurements r_1 and r_2.

The Lagrangian for the constrained minimization is:

$$\Lambda = \Delta r_1^2 + \Delta r_2^2 + \lambda(\Delta r_1 + \Delta r_2 - c) \tag{14}$$

The necessray conditions are given by:

$$\frac{\partial \Lambda}{\partial \Delta r_1} = 2\Delta r_1 + \lambda = 0 \tag{15a}$$

$$\frac{\partial \Lambda}{\partial \Delta r_2} = 2\Delta r_2 + \lambda = 0 \tag{15b}$$

$$\Delta r_1 + \Delta r_2 - c = 0 \tag{15c}$$

From (15), the minimial solution is:

$$\Delta r_1 = \Delta r_2 = \frac{c}{2} \tag{16}$$

Second, it is easy to see from the geometry of Fig. 2 that the range measurement prediction errors at $\hat{x}_A$, denoted by $\Delta r_1(\hat{x}_A)$ and $\Delta r_2(\hat{x}_A)$, are smaller than those at $\hat{x}_B$, denoted by $\Delta r_1(\hat{x}_B)$ and $\Delta r_2(\hat{x}_B)$. By sequence, the ML estimate occurs on the baseline and in the middle of two measurements, which is $\hat{x}_A$.

2.2 Analysis of ML Estimates

The following simulation compares four solutions, (i) ($\hat{x}$, $\hat{y}_+$) from (5a) and (5b) called "posi," (ii) ($\hat{x}$, $\hat{y}_-$) from (5a) and (5c) called "nega," (iii) ($\bar{x}$, $\bar{y} = 0$) from (9d) called "ave," and (iv) ($\hat{x}$, 0) from (9a) called "sect." In Case 3, the y-component of these solutions is set to zero.

Example 1. The two sensors are located at $\mathbf{s}_1$ = (100, 0) and $\mathbf{s}_2$ = (-100, 0), respectively. The target is at (10, 0). The range measurements are subject to independent zero-mean Gaussian noise with varaince $\sigma_1^2 = \sigma_2^2 = 2^2$.

Fig. 3 shows that the solutions "posi Δ" and "nega ∇" from the intersection of two circles are indeed the ML estimates. However, the ML estimates are driven by noisy range measurements (91.5981, 111.8818) off the baseline where the true target × lies. It also shows that the solution "ave ◊" is constrained on the baseline and it is closer to the truth (10.1418) than the x-coordinate of the ML estimates (10.3183).

When $r_1 + r_2 < 2x_1$, the circles do not intercept. In this case, it can be seen from the geometry that the the ML estimate occurs on the baseline. For the same simulation setting, the results for $r_1 + r_2 < 2x_1$ are shown for two sample runs in Figs. 4(a) and 4(b), respectively.

The circular intersection ("sect" o) and average ("ave" ◊) solutions are close to true target (×) but the "ave" is slightly closer than "sect." For the case that the circles do not intersect, the peak of the likelihood surface actually occurs along the baseline with $\hat{x}$ somewhere between the "sect" o and average "ave" ◊ solutions with $\hat{y} = 0$.

However, one of "posi" Δ and "nega" ∇ is closer to the true target (×) but it is difficult to tell which one, though. The mean value of "posi" Δ and "nega" ∇ is exactly the same as the "ave" ◊ as shown in (10), as depicted in Fig. 2.

Essentially, the ML estimate will be biased to lie on the baseline (when the target is on the baseline). As a result, the achieved localization performance can be finite despite the fact that the unbiased Cramer-Rao lower bound (CRLB) claims that the error is infinite. The ML performance is lower bounded by the "biased" CRLB.

Due to the intersecting circle geometries, the achievable localization accuracy gets worse as the baseline $2x_1$ grows to infinity because of the lack of curvature at the target location on the baseline. Lacking curvature, the intersecting circles would lead to larger uncertainties about the cross-range estimate. This effectively transforms the geometry from 2D to 1D.

3. Methods Adapted to Degenerate Geometry

Three methods for degenerate geometry are presented together with simulation analysis.

3.1 Method 1: 1D Solution for a 2D Scenario

For network-based sensing and targeting applications, it is more likely for a target to get close to or even cross the baseline of sensors. In such cases, the changes in GDOP may be significant, leading to degenerate cases.

Indeed, when a target is close to or crosses the baseline, the 2D solution is no longer applicable because the observation matrix is rank-deficient with near parallel LOS vectors. However, it is a quasi-1D scenario when near the baseline. Assume that two sensors are located at x_1 and x_2. The sensor range measurements are r_1 and r_2. The 1D estimate derived from the two measurements (7) is given by (8). The resulting position error is $\sigma_x = \sqrt{2}/2\sigma$, which is equivalent to having a GDOP of 0.707, the lowest of the 2D solution. A practical question then is when to switch from the 2D solution to the 1D solution.

As shown in Fig. 5, two sensors are at known locations $\mathbf{s}_1$ and $\mathbf{s}_2$. A target is at an unknown location $\mathbf{u}_0$, to be estimated by the two sensors with ranging measurements r_1

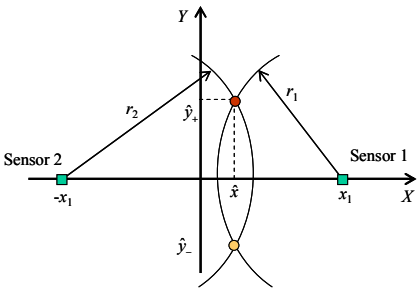

Fig. 1 Encounter Geometry with $r_1 + r_2 \geq 2x_1$

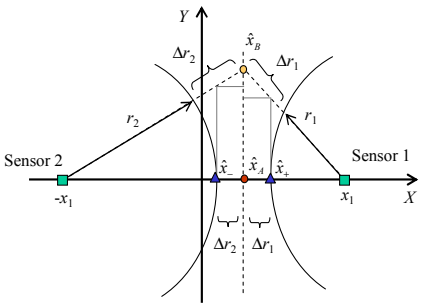

Fig. 2 Encounter Geometry with $r_1 + r_2 < 2x_1$

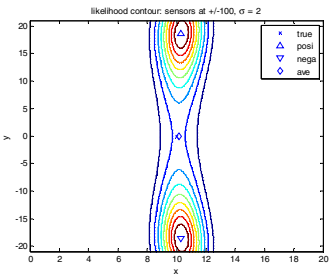

Fig. 3 Solutions when $r_1 + r_2 \geq 2x_1$

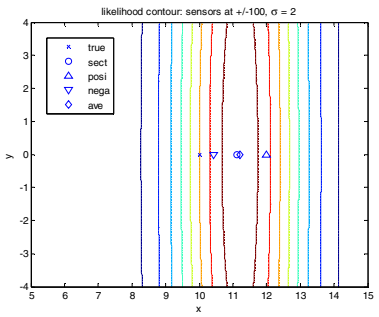

Fig. 4(a). Solutions when $r_1 + r_2 < 2x_1$

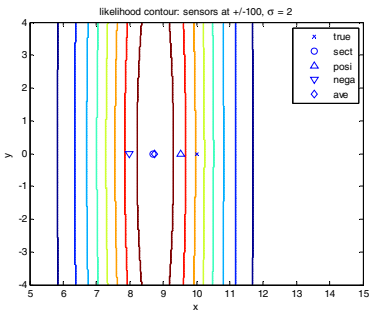

Fig. 4(b). Solutions when $r_1 + r_2 < 2x_1$

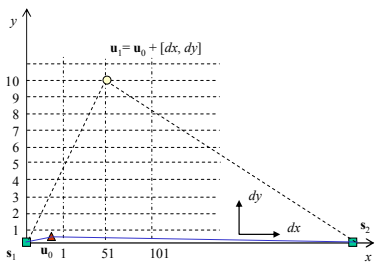

Fig. 5 Simulation Scenario

and r_2 having the measurement error variances σ_1^2 and σ_2^2, respectively. Note that the LOS vector is calculated from an initial estimate $\mathbf{u}_1$, which may be far away from the true state $\mathbf{u}_0$. A situation arises where $\mathbf{u}_0$ is very close to the baseline linking $\mathbf{s}_1$ and $\mathbf{s}_2$ so that the true lines of sight are close to parallel. The geometry has a very poor GDOP. However, since $\mathbf{u}_1$ has a large error, the resulting LOS vectors produce a GDOP, which is erroneously small, thus allowing for a solution. As the estimate gets to the true location, the estimated geometry is worsening. At this point, the poor geometry offers a clear sign for making a decision to switch from the 2D solution to the 1D solution. The process is illustrated with the following example.

Example 2. Referring to Fig. 5, there are two sensors located at $\mathbf{s}_1 = [0, 0]$ and $\mathbf{s}_2 = [1000, 0]$, respectively. The true target is located at $\mathbf{u}_0 = [50, 0.1]$. The measurement error is $\mathbf{R} = 1$. Without knowing the exact target location, the tracking algorithm initializes its state $\mathbf{u}_1 = \mathbf{u}_0 + [dx, dy]$ where dx and dy are the initial offset in x and y, respectively. The following values are considered:

$dy = 1, 11, 21, 31, 41, 51, 61, 71, 81, 91, 101$
$dx = 1, 101, 201, 301, 401$

As discussed above, an arbitrary initialization $\mathbf{u}_1$ may provide a reasonable value for the initial GDOP estimate. However, such an initial estimate, if far away from the true location, cannot provide a meaningful update despite its offering of a reasonable value for the initial GDOP estimate. Fig. 6 shows the GDOP as a function of dy for several dx. For small dy, the initial estimate $\mathbf{u}_1$ is close to the true value $\mathbf{u}_0$ near the x-axis and the corresponding estimated LOS vectors from $\mathbf{u}_1$ to $\mathbf{s}_1$ and $\mathbf{s}_2$ become parallel.

As shown in Fig. 7, for $dy > 10$, all initial estimates even with large dx are updated to within 25 to 50. However, for $dy < 10$, the updated state errors are larger than their initial errors even with small dx. Note that $dy = 10$ is the corner point where GDOP takes a sharp turn in values.

Fig. 7 indicates that direct application of the least squares solution in a poor geometry can lead to errors even worse than the initial errors.

Finally, note that this 1D solution introduces a bias because it ignores the distance off the baseline. Fig. 8 shows the position errors of the 1D solution (bias plus noise) compared to those of the 2D solution (GDOP times noise) for noise errors of $\sigma = 1$ and 10 m, respectively. As expected, the 1D solution error grows linearly, while the 2D solution error drops exponentially, with the distance from the baseline. The intersection point is about 55 m for $\sigma = 1$ m and 180 m for $\sigma = 10$ m, respectively. Depending on the separation of sensors and the measurement error variance σ, the intersection point may be determined and thus serves as the threshold for switch between the 1D and 2D solutions.

3.2 Method 2: Reduced-Order Least Squares Solution

Given the linearized observation equation with poor geometry, a reduced-order least squares solution may be used to obtain an otherwise unavailable solution. To start, we perform singular value decomposition (SVD) on the observation matrix as:

$$\mathbf{H} = \mathbf{U}\mathbf{S}\mathbf{V}^T \tag{17}$$

where $\mathbf{H}$ is an $m \times n$ matrix, $\mathbf{U}$ is an $m \times m$ orthonormal matrix, $\mathbf{S} = diag\{[\lambda_1, \ldots, \lambda_n]\}$ is an $n \times n$ diagonal matrix with the singular values λ_i arranged in a descending order, and $\mathbf{V}$ is an $n \times n$ orthonormal matrix.

The ordinary least square solution can be written as:

$$\Delta\mathbf{x} = \mathbf{V}\mathbf{S}^{-1}\mathbf{U}^T\mathbf{z} \tag{18}$$

where $\mathbf{S}^{-1} = diag\{[\lambda_1^{-1}, \ldots, \lambda_n^{-1}]\}$.

The solution is acceptable if the values of all λ_i^{-1} are on the similar order of magnitude. However, in poor geometry cases, numerical issues arise when some of λ_i^{-1} are off by two or more orders of magnitude.

The reduced-order least squares solution is to retain "good" singular values while discarding "bad" singular values. It applies a threshold testing as:

$$\left(\frac{\lambda_i}{\lambda_1}\right)^{-1} \begin{matrix} \text{Keep } i \\ \leq \\ > \\ \text{Discard } i \end{matrix} \tau \tag{19}$$

With the k largest singular values retained, the resulting solution is then written as:

$$\tilde{\mathbf{x}} = \mathbf{V}\tilde{\mathbf{S}}^{-1}\mathbf{U}^T\mathbf{z} \tag{20a}$$

$$\tilde{\mathbf{S}}^{-1} = diag\{[\lambda_1^{-1} \quad \cdots \quad \lambda_k^{-1} \quad 0]\} \tag{20b}$$

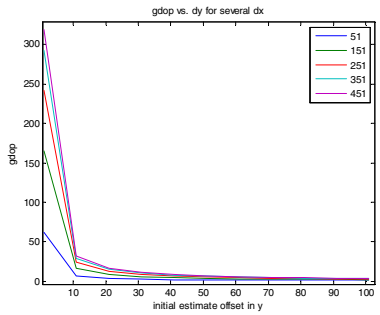

Fig. 6 GDOP as a Function of dy over dx

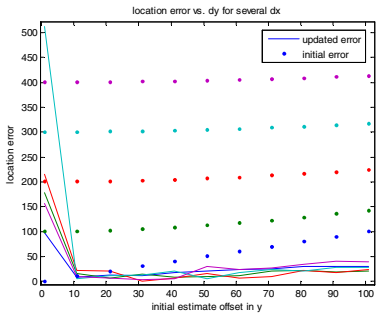

Fig. 7 Location Errors after One-Step Update

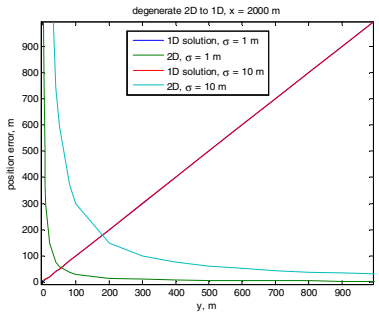

Fig. 8 Switch between 1D and 2D Solution

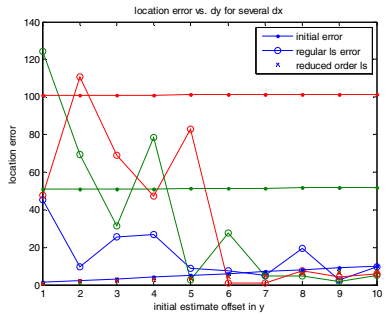

Fig. 9 Reduced-Order LS Errors after Update

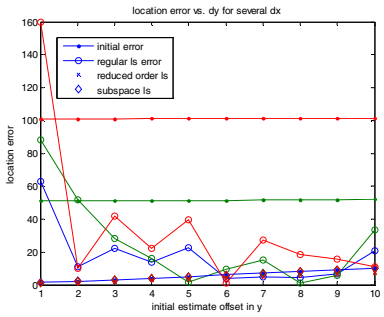

Fig. 10 Subspace LS Errors after Update

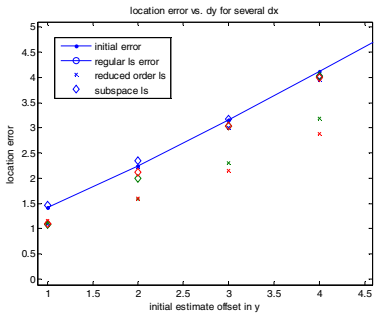

Fig. 11 Details of Fig. 10

Example 3. Continue with the previous example. Now the tracking algorithm initializes its target state $\mathbf{u}_1 = \mathbf{u}_0 + [dx, dy]$ where dx = 1, 51, 101 and dy = 1, 2, 3, 4, 5, 6, 7, 8, 9, and 10, respectively. Fig. 9 shows the location errors as a function of dy = 1 through 10 for dx = 1 (blue), 51 (green), and 101 (red).

For the regular LS solution, when $dy > 6$, the initial estimation errors (with dotted line marks •), even with large dx, are updated to within 10 (with circular line marks o). However when small $dy < 6$, the updated state errors (with circular line marks o) are larger than their initial errors (with dotted line marks •) even with small dx. Consistent with Fig. 7, Fig. 9 also indicates that direct application of the least squares solution in a poor geometry can lead to errors even worse than the initial errors.

The reduced-order least squares solutions (20) are shown in Fig. 9 as the cross points (×). They are all smaller than the initial estimates even in poor geometries. For dx = 1, the location error is dominated by dy. The error reduction with conventional LS solution (o) depends on dy, that is, no reduction for $dy < 6$ and some reduction for $dy > 6$. However, with the reduced-order LS, the error reduction (blue crosses), even though small, is consistent.

The error reductions are more pronounced for dx = 51 (green crosses) and 101 (red crosses) when $dy < 5$. For these poor geometry cases, the results provided by the reduced-order LS solution are remarkable, which provide much better error reduction along the direction in the x-axis than in the y-axis.

3.3 Method 3: Subspace Least Squares Solution

An alternative approach to obtaining the 1D solution for a 2D scenario is the subspace least squares solution applied to the linearized observation equation with poor geometry. To start, we decompose the original state space $\mathbf{x} \in \mathcal{X} = \mathcal{R}^n$ into two orthogonal subspaces with dimensions k and n-k, denoted by $\mathcal{A}$ and $\mathcal{B}$, respectively, such that $\mathcal{A} \oplus \mathcal{B} = \mathcal{X}$.

Assume that we have found a matrix $\mathbf{A}$ whose columns span the subspace of $\mathcal{A}$, that is, $\mathbf{A} \in \mathcal{A} = \mathcal{R}^{n\times k}$. Similarly, the columns of a matrix $\mathbf{B}$ span the subspace of $\mathcal{B}$, that is, $\mathbf{B} \in \mathcal{B} = \mathcal{R}^{n\times(n-k)}$. The original solution can now be written as:

$$\Delta\mathbf{x} = \mathbf{A}\Delta\mathbf{x}_A + \mathbf{B}\Delta\mathbf{x}_B \tag{21}$$

The linearized measurement equation can be written as:

$$\mathbf{z} = \mathbf{H}\Delta\mathbf{x} + \mathbf{n} \tag{22a}$$
$$= \mathbf{H}(\mathbf{A}\Delta\mathbf{x}_A + \mathbf{B}\Delta\mathbf{x}_B) + \mathbf{n} \tag{22b}$$
$$= \mathbf{HA}\Delta\mathbf{x}_A + \mathbf{HB}\Delta\mathbf{x}_B + \mathbf{n} \tag{22c}$$

If $\mathbf{B}$ is chosen such that $\mathbf{HB} \approx \mathbf{0}$, then

$$\mathbf{z} \approx \mathbf{HA}\Delta\mathbf{x}_A + \mathbf{n} \tag{23a}$$
$$\Delta\mathbf{x}_A = (\mathbf{A}^T\mathbf{H}^T\mathbf{HA})^{-1}\mathbf{H}^T\mathbf{A}^T\mathbf{z} \tag{23b}$$

More generally, following the approach of [2], we can rewrite (22b) (ignoring the noise term) as:

$$\mathbf{z} = \mathbf{H}\begin{bmatrix}\mathbf{A} & \mathbf{B}\end{bmatrix}\begin{bmatrix}\Delta\mathbf{x}_A \\ \Delta\mathbf{x}_B\end{bmatrix} \tag{24a}$$

$$\begin{bmatrix}\mathbf{A} & \mathbf{B}\end{bmatrix}^T\mathbf{H}\begin{bmatrix}\mathbf{A} & \mathbf{B}\end{bmatrix}\begin{bmatrix}\Delta\mathbf{x}_A \\ \Delta\mathbf{x}_B\end{bmatrix} = \begin{bmatrix}\mathbf{A} & \mathbf{B}\end{bmatrix}^T\mathbf{z} \tag{24b}$$

$$\begin{bmatrix}\mathbf{A}^T\mathbf{HA} & \mathbf{A}^T\mathbf{HB} \\ \mathbf{B}^T\mathbf{HA} & \mathbf{B}^T\mathbf{HB}\end{bmatrix}\begin{bmatrix}\Delta\mathbf{x}_A \\ \Delta\mathbf{x}_B\end{bmatrix} = \begin{bmatrix}\mathbf{A}^T\mathbf{z} \\ \mathbf{B}^T\mathbf{z}\end{bmatrix} \tag{24c}$$

Multiplying the first block of rows of (24c) by $\mathbf{B}^T\mathbf{HA}(\mathbf{A}^T\mathbf{HA})^{-1}$ and subtracting it from the second block of rows of (24c) (i.e., block Gaussian elimination) gives:

$$\begin{bmatrix}\mathbf{A}^T\mathbf{HA} & \mathbf{A}^T\mathbf{HB} \\ \mathbf{0} & \mathbf{G}\end{bmatrix}\begin{bmatrix}\Delta\mathbf{x}_A \\ \Delta\mathbf{x}_B\end{bmatrix} = \begin{bmatrix}\mathbf{A}^T\mathbf{z} \\ \mathbf{g}\end{bmatrix} \tag{25a}$$

where

$$\mathbf{G} = \mathbf{B}^T\mathbf{HB} - \mathbf{B}^T\mathbf{HA}(\mathbf{A}^T\mathbf{HA})^{-1}\mathbf{A}^T\mathbf{HB} \tag{25b}$$
$$\mathbf{g} = \mathbf{B}^T(\mathbf{I} - \mathbf{HA}(\mathbf{A}^T\mathbf{HA})^{-1}\mathbf{A}^T)\mathbf{z} \tag{25c}$$

Note that $\mathbf{G}$ is called the Schur complement of $\mathbf{A}^T\mathbf{HA}$. From (25a), it can be seen that:

$$\mathbf{G}\Delta\mathbf{x}_B = \mathbf{g} \tag{26a}$$
$$\mathbf{A}^T\mathbf{HA}\Delta\mathbf{x}_A = \mathbf{A}^T(\mathbf{z} - \mathbf{HB}\Delta\mathbf{x}_B) \tag{26b}$$

from which $\mathbf{x}_A$ and $\mathbf{x}_B$ can be found to obtain the full solution $\mathbf{x}$ with (21).

Clearly, the subspace least squares solution depends on how the two subspaces are chosen. For our 2D scenarios, we first perform an affine transformation that translates and rotates the coordinates such that $\mathbf{s}_1$ is at the origin of the

transformed coordinate system and $\mathbf{s}_2$ is along the x-axis. Construct the first basis from $\mathbf{s}_1$ and $\mathbf{s}_2$ as:

$$\mathbf{e}_1 = \frac{\mathbf{s}_2 - \mathbf{s}_1}{\|\mathbf{s}_2 - \mathbf{s}_1\|_2} \tag{27a}$$

Construct the second basis perpendicular to $\mathbf{e}_1$ as

$$\mathbf{e}_2 = \begin{bmatrix} 0 & -1 \\ 1 & 0 \end{bmatrix} \mathbf{e}_1 \tag{27b}$$

The affine transformation is given by

$$\xi = [\mathbf{e}_1 \quad \mathbf{e}_2]^T (\mathbf{x} - \mathbf{s}_1) \tag{27c}$$

In the new coordinate system, we can select the two orthogonal subspaces as

$$\mathbf{A} = \begin{bmatrix} 1 \\ 0 \end{bmatrix}, \qquad \mathbf{B} = \begin{bmatrix} 0 \\ 1 \end{bmatrix} \tag{28}$$

Denote the observation matrix by

$$\mathbf{H} = \begin{bmatrix} \mathbf{h}_1^T \\ \mathbf{h}_2^T \end{bmatrix} = \begin{bmatrix} h_{11} & h_{12} \\ h_{21} & h_{22} \end{bmatrix} \tag{29}$$

With (28) and (29), from (25a) and (25b), we have

$$\mathbf{G} = \frac{h_{22}h_{11} - h_{12}h_{21}}{h_{11}} \tag{30a}$$

$$\mathbf{g} = \frac{z_2 h_{11} - z_1 h_{21}}{h_{11}} \tag{30b}$$

As a result, the solution is given by

$$\Delta\mathbf{x}_B = \frac{z_2 h_{11} - z_1 h_{21}}{h_{22}h_{11} - h_{12}h_{21}} \tag{31a}$$

$$\Delta\mathbf{x}_A = \frac{z_1}{h_{11}} - \frac{h_{12}}{h_{11}} \Delta\mathbf{x}_B$$

$$= \frac{z_1}{h_{11}} - \frac{h_{12}}{h_{11}} \frac{z_2 h_{11} - z_1 h_{21}}{h_{22}h_{11} - h_{12}h_{21}} = \frac{z_1 h_{22} - z_2 h_{12}}{h_{22}h_{11} - h_{12}h_{21}} \tag{31b}$$

Example 4. Continue with the previous example where the tracking algorithm initializes its target state $\mathbf{u}_1 = \mathbf{u}_0 + [dx, dy]$ with dx = 1, 51, and 101 and dy = 1, 2, 3, 4, 5, 6, 7, 8, 9, and 10, respectively. Fig. 10 shows the location errors as a function of dy = 1 through 10 for dx = 1 (blue), 51 (green), and 101 (red).

Again for the regular LS solution, for dy > 5, the initial estimation errors (with dotted line marks •), even with large dx, are updated to within 10 (with circular line marks o). However, for small dy < 5, the updated state errors (with circular line marks o) are larger than their initial errors (with dotted line marks •), even with small dx. The results are consistent with Figs. 7 and 9, indicating that direct application of the least squares solution in a poor geometry can lead to errors even worse than the initial errors.

The subspace least squares solutions (26) as the diamond points (◊) are shown in Fig. 10 in comparison to the reduced-order least squares solutions (20) as the cross points (×). They are all smaller than the initial estimates even in poor geometries. The details are shown in Fig. 11.

For dx = 1 (the blue curves), the location error is dominated by dy. The error reduction with conventional LS solution (o) depends on dy, that is, no reduction for dy < 6 and some reduction for dy > 6. However, the error reduction of subspace LS (blue diamonds) is consistent as is the reduced-order LS solution (blue crosses).

As shown in Fig. 10, the error reductions are more pronounced for dx = 51 (green diamonds) and dx = 101 (red diamonds) when dy < 5. For these poor geometry cases, the results provided by the subspace LS solution are significant.

Fig. 10 also shows the location error reduction of the reduced-order LS, which seemly outperforms the subspace LS, both are superior over the conventional LS.

4. Parameter Analysis with Simulation

Several Monte Carlo simulations are conducted to obtain statistical results of the positioning performance as a function of design parameters. In the following figures, the curves (◊) marked as "MLE" in legends are for the MLE solution, which is a weighted non-linear least squares, calculated using (5). The curves (o) marked as "regular LS" in legends are actually iterated linear least squares, which entail starting with an initial estimate, linearizing the nonlinear measurement equations, solving for the errors, and updating the estimate. The curves (□) marked as "ave" in legends are calculated using (8). The curves (>) and (<) are for the reduced order and subspace solutions from Sections 3.2 and 3.3, respectively.

Example 5: Effect of Initialization. The two sensors are located at (500, 0) and (-500, 0), respectively. The target is at (50, 0.1). The range measurements are subject to independent zero-mean Gaussian noise with varaince $\sigma_1^2 = \sigma_2^2 = 2^2$. The initial position estimate is set as an offset from the true position at:

$$\Delta\hat{\mathbf{x}} = d[\cos\theta \quad \sin\theta] \tag{32}$$

where $\theta = 10^o$ and d is varied from 0 to 270.

The updated position errors (RMS) of various algorirthms as a function of the initial position errors are shown in Fig. 12. The RMS errors are calculated based on 1000 Monte Carlo runs. The ML estimate (◊) remains unaffected by the initial position estimate. This is understandable because it is solved from the closed form nonlinear equations without iteration from an initial condition.

The average estimate (□) is also not affected by the initial estimate because it is constrained to lie on the baseline.

The regular LS estimate (o) actually improves as the offset from the true position increases. This is because the observation matrix at a larger distance from the singular target location, albeit erroneous, produces a smaller GDOP.

However, this updating effectiveness flattens out and then gets worse due to large linearization errors.

With poor geometry, the iterated LS does not improve the estimate per iteration. For example, let the initial position error be 100. According to the figure, the updated position error is about 35. A second update with an initial error of 35 will increase the error back to 100. An oscillation behavior occurs, no convergence as one might desire.

The reduced order (>) and subspace (<) solutions exhibit an error that increases almost linearly with the initial position error. After one update, both methods can find a good estimate for the *x*-component while the y-component is not worse than that of the initial condition.

Example 6: Effect of Target Position with Fixed Initial Estimate Offset. In the second simulation, the target true position is at (50, *dy*) where *dy* is varied from 0 to 65. The initial position error off the true position is by a fixed amount of (40.3771, 7.1196). The results are shown in Fig. 13 where the RMS errors are calculated based on 1000 Monte Carlo runs.

Since the initial estimate is off the true position by a fixed amount and the true position moves away from the baseline, the geometry improves for the regular LS solution (o).

The ML solution (◊) also improves as the two circles crosses at an increased angle at the intersection point away from the baseline.

The average solution (□) stays on the baseline. That is why its error increases linearly with the true position offset from the baseline.

The reduced order (>) and subspace (<) solutions produce a good estimate for the *x*-component while their *y*-component is about the same as the initial condition. Since the initial estimate has a fixed offset about 7, the errors of both solutions therefore remain about the same.

Example 7: Effect of Target Position with Fixed Initial Estimate. Instead of a fixed offset from the true position, the initial condition itself is fixed at (200, 20) in the third simulation. Again, the target true position is at (50, *dy*) where *dy* is varied from 0 to 65. The results are shown in Fig. 14 where the RMS errors are calculated based on 1000 Monte Carlo runs.

The ML solution (◊) also improves as the two circles crosses at an increased angle at the intersection point away from the baseline. This trend will flat out and start to reverse when the two circles become parallel at a far distance.

Since the true position moves away from baseline, the regular LS solution (o) remains the same (over *dy* = 0 to 40) and then gets worse. This is because with a fixed initial condition and fixed sensors, the LOS vectors are constant, which is acceptable for small offsets from the baseline. At large offset, the LOS vectors no longer point to the correct directions. The LS solution errors increase due to initialization errors.

The average solution (□) stays on the baseline, which explains its error increases linearly with the true position offset from the baseline.

Since the reduced order (>) and subspace (<) solutions tie their *y*-component to the initial condition, which is 20, their errors first decreases as the true position *y* moves away from the baseline (*y* = 0) toward 20 and then increases linearly as the true position *y* moves away from 20 toward 100.

Discussions and Remarks

The study shows degenerate cases for conventional methods and suggests several methods to deal with such a geometry. Practical questions are how one knows *a priori* that the target is near the baseline and how one initializes the adapted methods. To solve this problem, we start with our knowledge about our sensor placement, based on which we know different regions in which different methods should be used if the target enters such regions.

Regardless where the true target is, the initial estimate and the sensor locations provide a perceived geometry. This perceived geometry, which may be totally wrong, shows a different degree of effectiveness in position error reduction for a linearized LS solution. For poor geometry, if the initial condition is closer to the true target, the updated solution may be steered farther away from the truth.

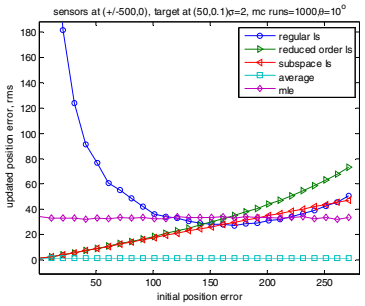

Fig. 12 Updated Position Errors (RMS) vs. Initial Error

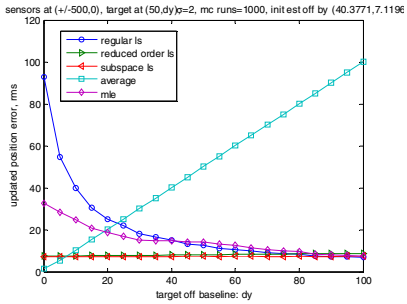

Fig. 13 Updated Position Errors (RMS) vs. Target Position (Fixed Initial Estimate Offset)

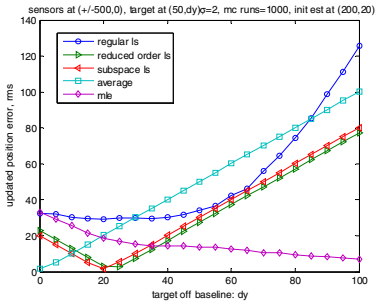

Fig. 14 Updated Position Errors (RMS) vs. Target Position (Fixed Initial Estimate)

Without an initial estimate, the nonlinear ML estimate from the closed-form solutions provides two performance bounds, one off the baseline (that is, one of the two circle intersect points) and one on the baseline (the average solution). However, the on-baseline solution (the best solution one can get) needs the prior information. The off-baseline solution is affected by a geometry factor.

The subspace method throws away the part in the direction perpendicular to the baseline while the reduced order method ignores the smaller singular value, both implying a near baseline encounter. However, both solutions are affected by the *y*-component of the initial condition. But they are no worse than the LS and are between the two ML estimates, depending on the initial condition and the actual offset.

If one has prior information that the target is on the baseline (or near the baseline), then one can insert the prior information in the MLE to get better results (if the prior information is correct). With the prior information, the Fisher information matrix can be made non-singular by reducing the order. Similarly, an iterative method that incorporates the prior (as pseduo measurements or constraints) may also be developed.

Scanning radars may provide coarse azimuth angles, which can be used to indicate a possible degenerate encounter. Monitoring GDOP is another way to assess the geometry.

5. Conclusions

For a given sensor configuration, the performance of target positioning and tracking algorithm depends, on one hand, on the sensor accuracy and, on the other hand, on the geometry of the given sensor configuration. Indiscriminate application of conventional least squares method may lead to large position errors caused by noise amplification due to poor GDOP. As a result, the performance measure can be used for processing algorithms selection and optimization for target positioning.

In this study, we investigated the MLE in degenerate geometry and proposed three approaches for such cases in a 2D scenario, namely, (i) geometrical 1D solution, (ii) reduced-order LS solution, and (iii) subspace LS solution, which were compared to the conventional least squares solution in computer simulations. There are three significant findings:

- Although the predicted LOS vectors can be chosen by an "arbitrary" initial estimate (that is, to produce a favorable GDOP), such an initialization may not necessarily lead to meaningful updates for next available measurements. In other words, the initialization has to be in the vicinity of the true location to reflect the geometry, albeit "poor," and to allow for measurement update to improve the solution.
- For a poor geometry, near-truth initialization leads to large errors with conventional methods due to noise amplification. Initialization with large errors would not provide much error reduction.
- The reduced-order solution outperforms other solutions even in poor geometries. As a result, the ratio of singular values (the largest vs. the smallest) of the observation matrix can be calculated and used as a test to determine when to apply the reduced-order solution as a means to switch from the full 2D solution to the degenerate 1D solution. The eigenvalue ratios are tied to GDOP.

The development of these methods adapted to degenerate cases can aid adaptive sensor management and active sensor placement strategies in target acquisition and track maintenance.

Future work includes extending the 2D solution and its degenerate 1D solution to higher dimensions and applying the methods for target tracking and other applications such as GPS in urban canyons. Additionally, testing the methods for operational scenarios with multiple targets and multiple sensors would require parameter selections between the realizable and degenerate cases as related to situational awareness of all targets in an area of interest.

Acknowledgement

Research supported in part under Contract No. FA8650-08-C-1407, which is greatly appreciated.

References

[1] D. Hertz, Sequential Ridge Regression, *IEEE Trans. on Aerospace and Electronic Systems*, AES-27 (3), May 1991, 571-574.

[2] M. Jaconsen, P.C. Hansen, and M.A. Saunders, "Subspace Preconditioned LSQR for Discrete Ill-Posed Problems," *BIT Numerical Mathematics*, 43, 975-989, 2003.

[3] R.J. Kelly, "Reducing Geometric Dilution of Precision Using Ridge Regression," *IEEE Transaction on Aerospace and Electronic Systems*, 26 (1), January 1990, 154-168.

[4] J.M. Mendel, *Discrete Techniques of Parameter Estimation*, Marcel Dekker, New York, 1973.

[5] R.M. Rifkin and R.A. Lippert, *Notes on Regularized Least Squares*, MIT-CSAIL-TR-025, CBCL-268, May 2007.

[6] C. Yang and E. Blasch, "Track Fusion with Road Constraints," *ISIF Journal of Advanced Information Fusion*, 2008.

[7] C. Yang and E. Blasch, "Kalman Filtering with Nonlinear State Constraints," *IEEE Trans. on Aerospace and Electronic Systems*, 2009.

[8] C. Yang, E. Blasch, and I. Kadar, "Geometric Factors in Target Positioning and Tracking," *Fusion2009*, Seattle, WA, July 2009.

[9] C. Yang, E. P. Blasch, J. Patrick, D. Qiu, and P. Douville, "Ground Target Track Bias Estimation Using Opportunistic Road Information," *IEEE NAECON*, 2010.